*Proceedings of the 21st ICSMGE, Vienna, Austria, 14 – 19 June 2026. Pistrol, Adam & Schweiger (eds.)*
*Published by: ÖGG, Austrian Society for Geomechanics, Salzburg, Austria, ISBN 978-3-9503898-4-5*
*https://doi.org/10.53243/ICSMGE2026-1084*

# Analysis of InSAR data and numerical modelling for the study of bridge-landslide interaction

**Alice Vitaletti**
*Department of Civil and Industrial Engineering, University of Pisa, Pisa, Italy, alice.vitaletti@phd.unipi.it*

Erica Cernuto, Diana Salciarini
*Department of Civil and Environmental Engineering, University of Perugia, Perugia, Italy*

ABSTRACT: Italy, due to its complex geological and geomorphological structure, is notoriously susceptible to landslide phenomena, which pose a significant threat to critical infrastructure. In recent years, the increasing number of infrastructure collapses caused by landslide has underscored the urgent need to better understand their impacts. This paper combines satellite-based Interferometric Synthetic Aperture Radar (InSAR) data and finite element (FEM) numerical modelling to analyse a case of interaction between a landslide and a bridge along a highway section in Liguria, focusing on a slow-kinematic landslide identified in the Inventory of Landslide Phenomena in Italy (IFFI). InSAR data, derived from the Copernicus European Ground Motion Service (EGMS), offered high-resolution spatial and temporal mapping of ground deformation. However, it lacks the capability to provide the underlying physical mechanisms of the phenomenon under varying loading conditions. To address this, FEM modelling was employed to simulate the mechanical behaviour of the landslide and its effect on slope stability and bridge deformations. Post-processing operations of InSAR data were conducted to obtain transverse and vertical real displacement components, aligning with the observed landslide movement, and facilitating the validation of the numerical model. FEM results indicated significant displacements in the downstream area of the slope, particularly at the base of the bridge piers located within the landslide area, due to the horizontal forces exerted on the foundation structure. The consistency between InSAR observations and numerical modelling results confirmed the effectiveness of the combined approach in identifying critical zones within the landslide movement. The study highlights the benefits and limitations of integrating FEM simulation with InSAR monitoring, proposing them as a tool to support hydrogeological risk management and decision-making regarding the infrastructure maintenance in landslide-prone regions.

KEYWORDS: InSAR, Numerical Modelling, FEM, Landslide, Bridge.

## 1 INTRODUCTION

The complex geological and geomorphological configuration of the Italian territory contributes to its high susceptibility to slope instabilities, including numerous active and potentially hazardous landslides (Bianchi & Salvati 2023; Haque, 2016). This predisposition is frequently triggered by natural factors, such as intense rainfall and seismic events, as well as by anthropogenic activities, including construction and slope re-profiling (Guzzetti et al. 2022; Salciarini et al. 2016; Segoni et al. 2014). In particular, the consequences of such phenomena can be especially severe when they affect critical infrastructure, as evidenced by the recent increase in collapses and structural damage (Gabrieli et al. 2024; Salciarini et al. 2024a). This growing susceptibility underscores the need for more in-depth investigations and reliable tools to monitor, predict, and manage landslide-related risks.

While traditional in situ methods – such as inclinometers, piezometers, and topographic surveys – remain essential for slope monitoring, they are often limited by high costs, complex implementation, and restricted spatial coverage, which reduce their effectiveness in extensive or inaccessible areas (Mazzella 2021). Conversely, Interferometric Synthetic Aperture Radar (InSAR) has proven to be an effective tool for mapping and monitoring ground deformations, offering wide-area coverage and frequent revisit times, with millimetric precision (Calvello et al. 2016; Casagli et al. 2016; Herrera et al. 2010). The development of advanced multi-interferogram approaches, such as Permanent Scatterer Interferometry (PS-InSAR), has further enhanced the ability to monitor slow-moving landslides, allowing for the assessment of their activity and the detection of displacement anomalies, at both regional and local scales (Bianchini et al. 2013; Cigna et al. 2013).

Nevertheless, the accuracy of InSAR data remains limited by its capacity to detect ground deformations only along the sensor's line of sight (LOS). Moreover, this technique does not provide physical insights into slope evolution or the response of affected structures under complex loading conditions. In this context, numerical methods such as Finite Element Modelling (FEM) address these limitations by simulating the full-scale landslide behaviour and the mechanical response of both slope and interacting structures (Castaldo et al. 2014; Cernuto et al. 2026; Salciarini et al. 2024b). However, FEM analysis requires prior knowledge of soil geotechnical parameters, which are often unavailable or difficult to obtain in practice.

Although the combination of InSAR and FEM has shown promising results in monitoring landslides in open-pit mines and urbanised hillslopes (Ma et al. 2021; Zhou et al. 2016), its application to the study of bridge-landslide interactions remains relatively unexplored, with only a few recent contributions in this field (e.g., Cernuto et al. 2025; Farneti et al. 2022).

Therefore, this study investigates potential and limitations of a coupled InSAR-FEM approach for analysing the behaviour of a landslide partially interacting with a bridge, inspired by a real-world case along the Ligurian highway. The objective is to provide a valuable tool to support infrastructure managers in planning maintenance activities and managing the landslide-related hydrogeological risk.

## 2 CASE STUDY

The study area is situated along the Ligurian section of the A12 highway, between Sestri Levante (GE) and Ceparana (SP), in Italy. According to the Inventory of Landslide Phenomena in Italy (IFFI), this region is highly susceptible to landslides, some of which directly affect the infrastructure along the highway network. To achieve the objective of the study, interferometric data from the Copernicus "European Ground Motion Service" (EGMS) were consulted. This service provides free and open access to InSAR data, enabling high-resolution monitoring of ground displacements using Sentinel-1 acquisitions, processed in both ascending and descending orbital geometries, typically updated every six days across participating European countries. Specifically, the datasets used cover the period from January

2018 to December 2022. The data, overlaid on an orthophoto map (Figure 1), include average annual deformation velocities (in mm/year) of the measurement points – so called Permanent Scatterers (PS) – along the sensor's line of sight (LOS), as well as the time series of displacements starting from the beginning of the monitoring period.

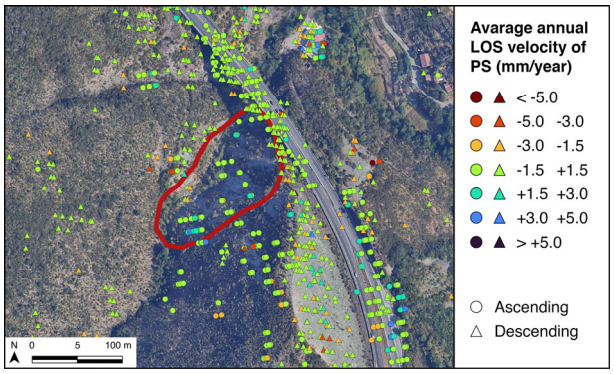


Figure 1. Case study orthophoto displaying the average annual LOS velocity of PS (in mm/year) in the two orbital geometries and landslide-affected area boundary (in red).

The analysis of InSAR data distribution focused on landslides with a significant areal extent (> 10,000 m²) that interact, either fully or partially, with critical infrastructure. Overall, the spatial distribution of radar targets within the landslide-affected areas varied across the highway section.

A major limitation in the application of satellite-based techniques to landslide monitoring is the inherently low density of PS in vegetated areas, where landslides typically occur and seasonal variations and wind exposure affect the radar signal over time. This variability limits the capacity of InSAR data to accurately represent landslide kinematics, thereby complicating their interpretation, especially when compared to information derived from in situ monitoring techniques.

Given the aim of this work, the proposed approach was applied to a case study located along the Ligurian highway, where a landslide classified by IFFI, covering approximately 12,122 m², partially interacts with a bridge situated on a moderately steep slope facing north-west (Figure 2). Further details can be found in Vitaletti et al. (2025). Compared to other cases analysed along the same highway section, InSAR data revealed an appreciable density (about 0.010 PS/m²) and a relatively homogeneous distribution of PS within the landslide body, enabling accurate mapping and assessment of the slope instability. Specifically, the average annual LOS velocity is generally stable (±1.5 mm/year), with peak values reaching up to +3 mm/year in descending geometry. It is worth noting that positive velocity values indicate movement towards the sensor, while negative values indicate motion away from it (Figure 1).

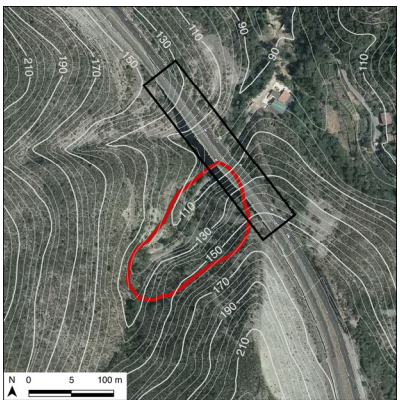


Figure 2. Case study orthophoto displaying the iso-elevation lines, the landslide-affected area boundary (in red), and the bridge (in black).

## 3 PROPOSED APPROACH

This study presents a coupled approach that combines numerical modelling with InSAR observations to investigate the effects of a landslide on partially interacting bridge foundations. Finite Element Method (FEM) simulations were performed using Plaxis 3D to assess slope stability and the structural response of the bridge foundations under hydro-mechanical loading conditions. The FEM computations enabled a full-scale simulation of the landslide evolution, providing valuable insights into the actual displacement direction. The results of the numerical analysis informed the definition of the local reference system adopted for interpreting the InSAR-derived displacements, thereby offering a physical basis for the assumption used in estimating the two-dimensional displacement field. In parallel, satellite data were post-processed to estimate the transverse and vertical components of the actual displacement, within a local reference system aligned with the landslide phenomenon. This analysis provided further insights into landslide-induced deformations and supported the reliability of the numerical model through comparison with the actual displacement patterns. The combination of numerical modelling and satellite observations enhanced the interpretation of the landslide behaviour and facilitated the identification of potentially susceptible areas, offering a predictive tool for infrastructure management and risk mitigation strategies.

### 3.1 *Finite element modelling*

The three-dimensional model, measuring 450 × 450 m with a height of 220 m, was implemented to simulate the rotational sliding behaviour of the landslide, which extends 175 m in length and 80 m in width, with a maximum sliding surface depth of 15 m (Figure 3). The sliding surface was determined through preliminary numerical analyses based on the strength reduction (phi-c reduction) method in Plaxis 3D, in which soil strength parameters are proportionally reduced until failure occurs, thus revealing the critical failure surface corresponding to the depth of about 15 m (Brinkgreve et al. 2016; Kupka et al. 2009).

The numerical model includes three distinct soil regions representing the stable soil, the landslide volume, and the sliding surface (Figure 4). For all regions, the Hardening Soil (HS) constitutive model was adopted (Schanz et al. 1999), which accounts for the progressive reduction in stiffness under primary deviatoric stress while developing irreversible plastic deformation.

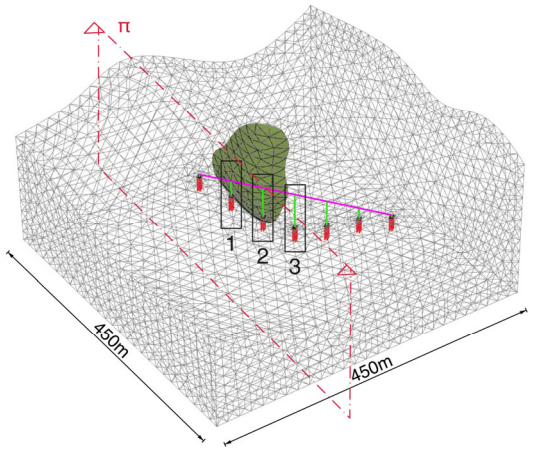


Figure 3. 3D numerical model, including the soil volume and the bridge structure, discretised into finite elements (mesh). Numbers 1 to 3 refer to the pier numbering.

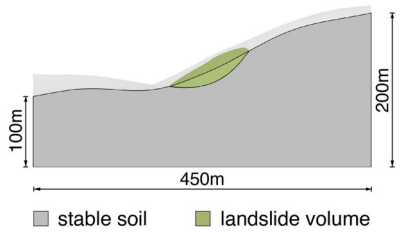

Figure 4. Section plane $\pi$ of the 3D numerical model.

A coarse-grained soil type was defined according to the geological profiles available for the study area. Owing to the lack of site-specific investigation data, the soil was assumed to be homogeneous, with the same physical and mechanical properties assigned to both the altered layer and stable soil, except for the shear strength parameters, which were assumed under residual conditions. To address the uncertainty associated with the absence of in-situ data, a sensitivity study based on back-analysis was performed to calibrate these parameters for both the stable soil and landslide volume, involving the independent variation of cohesion ($c'$) and friction angle ($\varphi'$) within ranges reported in the literature (Duncan & Wright 2005; Terzaghi et al. 1996). These analyses aimed to obtain global safety factors representative of a limit equilibrium condition for the slope, thereby ensuring a configuration consistent with the kinematic behaviour of the investigated mechanism. Stiffness parameters governing the HS model behaviour were defined according to soil type. The reference secant stiffness modulus ($E_{50}^{ref}$), set at 30.00 × 10³ kN/m², was selected based on the range proposed by Schanz et al. (1999). Using empirical relationships from the literature (Brinkgreve et al. 2024), the tangent stiffness ($E_{oed}^{ref}$) and the unloading/reloading stiffness ($E_{ur}^{ref}$) were derived, with values of 36.01 × 10³ kN/m² and 110.80 × 10³ kN/m², respectively. These same stiffness values were also assigned to the sliding surface, while the cohesion and friction angle were reduced to represent residual conditions and reproduce the sliding of the unstable volume along the failure surface (Table 1).

Table 1. Strength parameters assigned to different soil regions.

| Parameter | Stable soil | Landslide volume | Sliding surface | Unit |
|---|---|---|---|---|
| Cohesion ($c'$) | 35 | 25 | 5 | kN/m$^2$ |
| Friction angle ($\varphi'$) | 35 | 28 | 26 | ° |

The numerical model was completed by including the bridge, which partially interacts with the landslide-affected area. The structure consists of six spans, with a total deck length of 243 m. Since the primary objective of this study is to investigate the interaction between the landslide and the bridge foundations, simplifications were introduced for the superstructure. Specifically, the piers were modelled as linear elastic beams, and the deck as a single beam with a simply supported scheme.

The foundation system comprises a group of six reinforced concrete piles, each with a diameter of 1 m and an embedment depth of 20 m, spaced at three times the diameter and connected by a 0.8 m thick foundation slab (Figure 5). Piles were modelled as embedded beam elements, with the soil-structure interaction simulated through special interface elements. This includes a linearly elastic skin resistance ($T_{skin}$) along the pile shaft and a foot resistance ($F_{max}$) of 10 × 10³ kN/m.

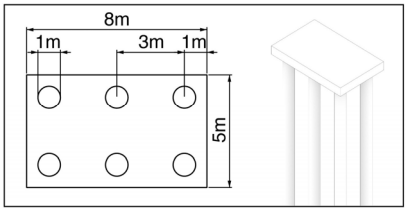

Figure 5. Bridge foundation structure.

The groundwater level was assumed at a depth of 7.5 m below ground level, approximately midway through the sliding surface, to account for pore water pressure effects on slope stability and foundation response.

The FEM analysis consisted of an initial stress generation phase using gravity loading, followed by a plastic analysis to simulate elasto-plastic deformations, and a safety calculation based on the phi-c reduction method to estimate the global safety factor.

### 3.2 *InSAR data post-processing*

InSAR observations are inherently limited to capturing the one-dimensional projection of the three-dimensional movement along the sensor's line of sight, which may not accurately represent the actual deformation pattern. This limitation is particularly critical in landslide scenarios, where movement predominantly occurs in the horizontal direction. In such cases, displacements may be significantly underestimated, or entirely undetected when the movement is perpendicular to the LOS. Therefore, to improve the interpretability of InSAR data, it is essential to project the LOS-derived measurements onto real deformation directions, allowing for the estimation of actual displacement components.

Ideally, this requires spatially and temporally coincident observations, meaning that the same measurement point is observed simultaneously from different acquisition geometries. As this condition is rarely achieved in practice, datasets must be resampled and temporally aligned through post-processing operations.

In this study, a grid-based resampling method was adopted, following the approach proposed by Proietti et al. (2009). The study area was divided into of 60 × 60 m cells, and for each cell, the centroid – referred to as "synthetic PS" – was assigned the average LOS velocity of all PS contained within it, for both ascending and descending geometries and across all acquisition dates (Figure 6). Furthermore, temporal interpolation was also performed over the common monitoring interval (06/01/2018-22/12/2022). The combination of datasets from both geometries resulted in a spatially uniform distribution of synthetic PS, providing a representative overview of the landslide-related deformation.

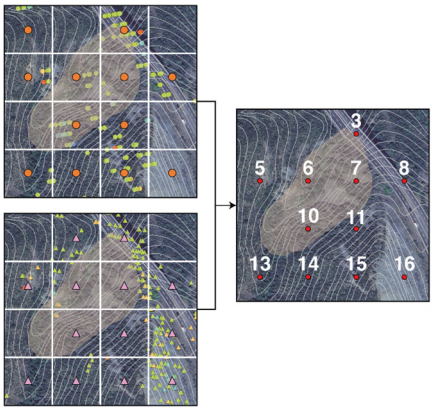

Figure 6. Schematic representation of the combination of ascending (top) and descending (bottom) datasets.

Reconstructing the 3D displacement vector requires at least three independent observations from distinct LOS geometries. However, with only two available geometries from the same satellite, the system is underdetermined and admits infinite solutions. In this context, this study adopted an approach aligned with Farneti et al. (2022), based on a local reference system (L, T, V) fixed to the deformation phenomenon. In this system, the longitudinal (L) axis is parallel to the iso-elevation lines of the landslide-affected slope, while the transverse (T) direction aligns with the horizontal direction of displacement, directed downslope (Figure 7).

More generally, the actual displacement vector, $d$, can be derived from the LOS measurement, $d_{LOS}$, using the vector projection equation:

$$d = \frac{d_{LOS}}{u_d \cdot u_{LOS}} \quad (1)$$

where $u_d$ and $u_{LOS}$ are the unit vectors defining the directions of the actual and LOS displacement vectors, respectively, in the global coordinate system (E, N, V).

Using the local reference system, $d_{LOS}$ can be expressed as a linear combination of the actual displacement components $d_L$, $d_T$, $d_V$. This formulation leads to a linear system of two equations and three unknowns, based on the two available LOS measurements:

$$d_{LOS} = Ad \quad (2)$$

where:

$$d_{LOS} = \begin{cases} d_A \\ d_D \end{cases}$$

$$A = \begin{bmatrix} \sin\theta_A \sin(\alpha_A + \varphi) & \sin\theta_A \cos(\alpha_A + \varphi) & \cos\theta_A \\ \sin\theta_D \sin(\alpha_D + \varphi) & \sin\theta_D \cos(\alpha_D + \varphi) & \cos\theta_D \end{bmatrix}$$

$$d = \begin{cases} d_L \\ d_T \\ d_V \end{cases}$$

where $\theta$ is the incidence angle of the LOS, and $\varphi$ is the angle defining the transverse direction of the actual displacement in the horizontal plane with respect to the global reference system (Figure 7).

Given the underdetermined nature of the system, it was necessary to introduce an assumption regarding the direction of the landslide movement. In this study, the deformation direction derived from the FEM simulations informed the orientation of the local reference system and enabled the estimation of the two-dimensional displacement field. The numerical results revealed that the actual movement occurred mainly along the downslope direction – nearly parallel to the bridge – which was assumed to represent the transverse axis of the local reference system (L, T, V). This supported the assumption of negligible longitudinal movement ($d_L = 0$) and justified the projection onto the (T, V) plane. The assumption is consistent with gravity-driven phenomena (e.g., glacier movement, slope instability), where movement primarily occurs downslope and longitudinal displacements, parallel to the iso-elevation lines of the slope, are negligible (Brouwer et al. 2021).

Under this condition, LOS measurements can be directly projected onto the (T, V) deformation plane. By removing the terms related to the assumed null longitudinal component ($d_L = 0$), the system simplifies to two equations in two unknowns. The resulting 2D displacement vector, $\hat{d} = (d_T, d_V)$, is then obtained by inverting Equation (2):

$$\hat{d} = B^{-1} d_{LOS} \quad (3)$$

where B is the 2×2 submatrix of the original matrix $A$, derived by excluding the column corresponding to $d_L$.

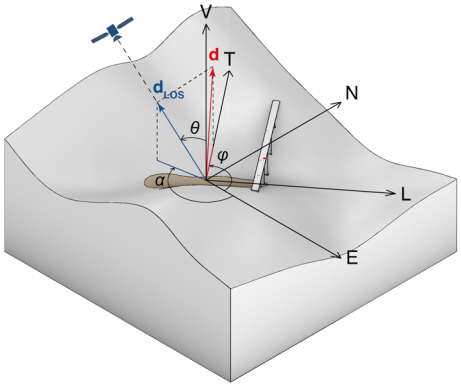


Figure 7. Representation of the displacement vector and its projection along the LOS in the local reference system (L, T, V).

## 4 RESULTS

The FEM analysis revealed that the highest total displacements ($|u|$) are mainly concentrated in the downslope portion of the landslide-affected area, reaching peak values of approximately 4.6 cm. Additional deformations were also observed in the upslope portion of the slope, likely due to pore water pressures, where total displacements reached about 2 cm (Figure 8).

The computed global safety factor ($\Sigma Msf$) assumed a value of 1.168, indicating that the slope is close to the limit equilibrium condition. Numerical results confirmed a rotational sliding mechanism of the landslide volume downslope, with plastic deformations affecting some of the bridge foundations.

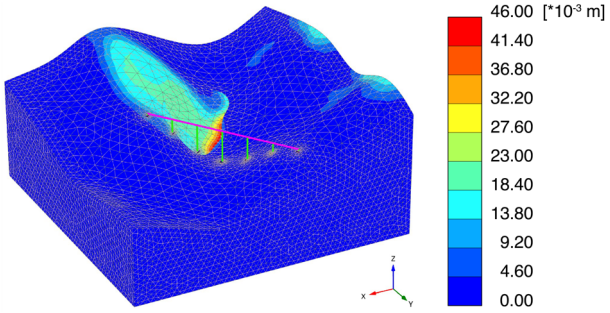


Figure 8. 3D numerical model showing the total displacements |u| resulting from the FEM analysis.

In addition, displacements were examined with respect to the global reference system (x, y, z) at the selected control points located at the top (pier-deck node) and base (pier-foundation node) of Piers 1 and 2 – both situated within the landslide body – and Pier 3, located outside the unstable area (Figure 3). To evaluate the structural response to the landslide in quantitative terms, only the horizontal displacement components ($u_x$ and $u_y$) were considered, consistent with the dominant direction of landslide phenomena, which are primarily characterised by horizontal deformations.

Piers 1 and 2 exhibited notable downslope displacements at the base due to the thrust exerted by the landslide volume on the foundations. Conversely, the base of Pier 3 showed smaller, upslope-oriented movements, likely due to the restraining effect provided by the structure (Table 2).

The deck undergoes compression and, behaving as a rigid element, slightly resists the forward movement of the heads of Piers 1 and 2. However, it is important to note that these results may be influenced by the simplified assumptions adopted in the model, which led to examining the superstructure under the most critical configuration.

Table 2. Horizontal displacements at selected control points.

| Control points | $u_x$ | $u_y$ | Unit |
|---|---|---|---|
| Top Pier 1 | -5.10 | 2.49 | mm |
| Base Pier 1 | -3.80 | 4.97 | mm |
| Top Pier 2 | -3.37 | 1.90 | mm |
| Base Pier 2 | -2.94 | 5.65 | mm |
| Top Pier 3 | -1.07 | 0.10 | mm |
| Base Pier 3 | 1.86 | -0.85 | mm |

In parallel with the numerical simulations, InSAR data post-processing enabled the estimation of time series for the transverse and vertical components of the actual displacement at the synthetic PS within the study area.

The results for vertical displacement ($d_V$) show that the synthetic PS in cell 3, located along the bridge, undergoes periodic deformation consistent with the seasonal temperature variations – subsiding during colder months and rising during warmer periods. In contrast, the synthetic PS located within the vegetated landslide area (cells 6, 7, 10, 11, and 14) does not exhibit clear seasonal pattern, but instead display a generally stable trend with a slight linear subsidence, compatible with the overall downslope movement of the landslide (Figure 9).

The transverse displacement ($d_T$) time series display greater temporal variability, particularly within the vegetated landslide area, likely due to temporal decorrelation effects caused by vegetation. These signal fluctuations are reflected in the anomalous values that deviate from the expected trend. Nevertheless, when disregarding these anomalies, a linear trend of progressive uplift is observed, consistent with the direction of landslide movement. One notable exception is evident in cell 6, where the transverse displacement trend appears inverted, suggesting movement opposite to the expected direction. This discrepancy may result from the inclusion of target points from descending geometry outside the landslide-affected area during the resampling process, which may have captured unrelated ground deformations (Figure 10).

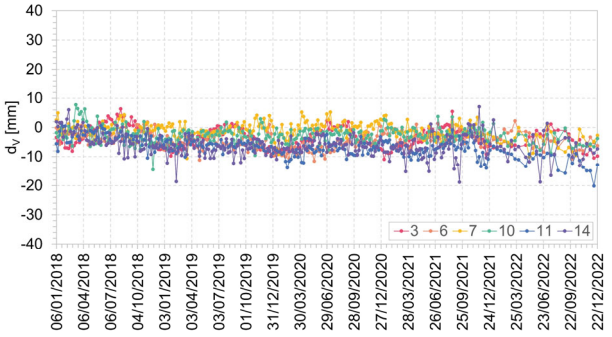

Figure 9. Time series of vertical displacement component.

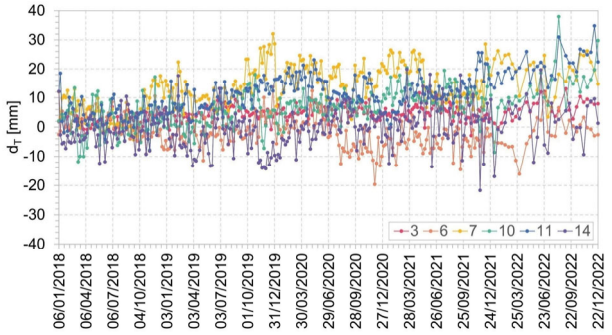

Figure 10. Time series of transverse displacement component.

While InSAR data post-processing enabled the estimation of the actual displacement components, these results reflect a transient analysis limited to the monitoring period (2018-2022). In contrast, the FEM was conducted as a steady-state analysis, with results representing final deformations associated with the new equilibrium configuration of the system. Due to these methodological differences, a quantitative comparison was not feasible.

Nevertheless, a qualitative comparison revealed consistent deformation patterns. Synthetic PS located upstream of the landslide-affected area (cells 7 and 11) exhibited significant horizontal displacements aligned with the landslide kinematics, supporting the model's ability to identify susceptible areas. A similar agreement was observed for the minor displacements in upslope sectors (cells 10 and 14). Conversely, discrepancies were noted in grid cell 6, where InSAR-derived displacements diverged from the expected trend, highlighting the inherent limitations of satellite-based monitoring.

Overall, despite the intrinsic differences between the two approaches, the combination of InSAR observations and numerical modelling enhances the interpretation of satellite-derived measurements and strengthens the reliability of the FEM in identifying areas susceptible to instability. This highlights the added value of coupling satellite data with numerical simulations in improving both the understanding of full-scale landslide processes and the evaluation of slope instability affecting critical infrastructure.

## 5 CONCLUSIONS

This study investigated the effects of a landslide on bridge foundations by combining Finite Element Modelling (FEM) with satellite-based data analysis, focusing on a case inspired by a real-world bridge-landslide interaction scenario along the Ligurian section of the A12 highway. A preliminary large-scale assessment enabled the distribution of InSAR data to be evaluated in relation to mapped landslides across the study area.

A 3D numerical model was developed to simulate a rotational landslide partially affecting a bridge on a moderately steep slope under hydraulic loading conditions. FEM results highlighted notable displacements in the downslope portion of the landslide, as well as additional ground movements upslope, confirming the expected rotational mechanism and suggesting a slope stability condition close to the limit equilibrium. The analysis also revealed significant deformations at the base of the piers located within the unstable volume, attributed to horizontal thrust exerted on the bridge foundations.

In parallel, InSAR datasets were post-processed through spatial and temporal interpolation, resampled over a 60 × 60 m grid, and projected within a local reference system (L, T, V) fixed to the landslide. This procedure allowed for the estimation of time series for the transverse and vertical components of the actual displacement, exhibiting deformation patterns consistent with the expected landslide behaviour.

The qualitative comparison between the numerical and satellite-derived results confirmed overall consistency in the deformation trends, thereby supporting the effectiveness of the numerical model in identifying susceptible areas. Nevertheless, discrepancies observed at the synthetic PS within grid cell 6 underscored the intrinsic limitations of InSAR measurements for monitoring ground deformation in complex, landslide-prone regions.

In conclusion, this study has shown that combining FEM modelling with satellite-based monitoring can enhance both the reliability of numerical predictions and the interpretation of InSAR data. This approach proves particularly valuable in large-scale infrastructure contexts, especially where ground-

based information may be unavailable, offering support for risk assessment and maintenance planning by highway managers.

## 6 ACKNOWLEDGEMENTS

This study was supported by FABRE – "Research consortium for the evaluation and monitoring of bridges, viaducts and other structures" (www.consorziofabre.it/en). Any opinion expressed in the paper does not necessarily reflect the view of the funder. Additionally, it was supported by the project "Methodological Approaches for RIsk assessment in the framework of landslide-bridge IntEraction (MARIE)".

## 7 REFERENCES

Bianchi, C., Salvati, P. 2023. *Rapporto Periodico sul Rischio posto alla Popolazione italiana da Frane e Inondazioni. Anno 2022*. Istituto di Ricerca per la Protezione Idrogeologica (IRPI).

Bianchini, S., Herrera, G., Mateos, R., Notti, D., Garcia, I., Mora, O., et al. 2013. Landslide Activity Maps Generation by Means of Persistent Scatterer Interferometry. *Remote Sensing,* 5, 6198-6222.

Brinkgreve, R.B.J., Engin, E., Swolfs, W.M. 2024. *Material models manual 3D*. Delft: Plaxis bv.

Brinkgreve, R. B. J., Kumarswamy, S., Swolfs, W. M., Waterman, D., Chesaru, A., Bonnier, P. G. 2016. *PLAXIS 2016*. PLAXIS bv, the Netherlands, 1-16.

Brouwer, W.S., and Hanssen, R.F. 2021. An Analysis of Insar Displacement Vector Decomposition Fallacies and the Strap-Down Solution. 2021. In: IEEE, *International Geoscience and Remote Sensing Symposium,* 10, 2927-2930.

Calvello, M., Peduto, D., Arena, L. 2016. Combined use of statistical and DInSAR data analyses to define the state of activity of slow-moving landslides. *Landslides,* 14, 473-489.

Casagli, N., Cigna, F., Bianchini, S., Hölbling, D., Füreder, P., Righini, G., et al. 2016. Landslide mapping and monitoring by using radar and optical remote sensing: Examples from the EC-FP7 project SAFER. *Remote Sensing Applications: Society and Environment,* 4, 92-108.

Castaldo, R., Tizzani, P., Lollino, P., Calò, F., Ardizzone, F., Lanari, R., et al. 2014. Landslide Kinematical Analysis through Inverse Numerical Modelling and Differential SAR Interferometry. *Pure and Applied,* 172, 3067-3080.

Cernuto, E., Salciarini, D., Ubertini, F., Giardina, G. 2025. Landslide-Bridge Interaction: A combined approach based on InSAR data and numerical modelling. *International Journal of Disaster Risk Reduction*, 126, 105568.

Cernuto, E., Vitaletti, A., Salciarini, D. 2026. Effect of the Relative Bridge-Landslide Orientation on the Seismic Behaviour of a Bridge. *Soil Dynamics and Earthquake Engineering*, 200, 109899.

Cigna, F., Bianchini, S., Casagli, N. 2013. How to assess landslide activity and intensity with Persistent Scatterer Interferometry (PSI): the PSI-based matrix approach. *Landslides,* 10, 267-283.

Duncan, J.M., Wright, S.G. 2005. *Soil Strength and Slope Stability*. John Wiley and Sons, Inc.

Farneti, E., Cavalagli, N., Costantini, M., Trillo, F., Minati, F., et al. 2022. A method for structural monitoring of multispan bridges using satellite InSAR data with uncertainty quantification and its pre-collapse application to the Albiano-Magra Bridge in Italy. *Structural Health Monitoring,* 22, 353-371.

Gabrieli, F., Gibin, F., Brezzi, L., Cernuto, E., Lupatelli, A., Salciarini, D., et al. 2024. Lessons from international case studies on bridge-slide interaction problems. *Procedia Structural Integrity,* 62, 506-513.

Guzzetti, F., Gariano, S.L., Peruccacci, S., Brunetti, M.T., Melillo, M. 2022. Rainfall and landslide initiation. *Rainfall,* 427-450.

Haque, U., Blum, P., da Silva, P.F., Andersen, P., Pilz, J., Chalov, S.R., et al. 2016. Fatal landslides in Europe. *Landslides,* 13, 1545-1554.

Herrera, G., Notti, D., García-Davalillo, J.C., Mora, O., Cooksley, G., Sánchez, M., et al. 2010, Analysis with C- and X-band satellite SAR data of the Portalet landslide area. *Landslides*, 8, 195-206.

Kupka, M., Herle, I., Arnold, M. 2009. Advanced calculations of safety factors for slope stability. *International Journal of Geotechnical Engineering*, 3, 509-515.

Ma, P., Cui, Y., Wang, W., Lin, H., Zhang, Y. 2021. Coupling InSAR and numerical modeling for characterizing landslide movements under complex loads in urbanized hillslopes. *Landslides*, 18, 1611-1623.

Mazzella, D. 2021. *Linee guida SNPA.* 32/2021. Roma: ISPRA.

Proietti, C., Righini, G., Cigna, F., Pancioli, V., Casagli, N. 2009. *Linee Guida per l'analisi di dati interferometrici satellitari in aree soggette a dissesti idrogeologici*. Roma: MATTM.

Salciarini, D., Volpe, E., Kelley, S.A., Brocca, L., Camici, S., Fanelli, G., et al. 2016. Modeling the Effects Induced by the Expected Climatic Trends on Landslide Activity at Large Scale. *Procedia Engineering*, 158, 541-545.

Salciarini, D., Cernuto, E., Capati, G., Dezi, F., Brezzi, L., Gibin, F., et al. 2024a. Landslide-bridge interaction: Insights from an extensive database of Italian case studies. *International Journal of Disaster Risk Reduction,* 114, 104983.

Salciarini, D., Pauselli, D., Cernuto, E., Boco, G., Ubertini, F. 2024b. Analysis of the interaction of a landslide with viaduct foundations under static and dynamic conditions. *Procedia Structural Integrity,* 62, 514-521.

Schanz, T., Vermeer, P.A., Bonnier, P.G. 1999. The hardening-soil model: Formulation and verification. In: *Beyond 2000 in Computational Geotechnics,* 281-290. Rotterdam.

Segoni, S., Rossi, G., Rosi, A., Catani, F. 2014. Landslides triggered by rainfall: A semi-automated procedure to define consistent intensity-duration thresholds. *Geosciences*, 63, 123-131.

Terzaghi, K., Peck, R.B., Mesri, G. 1996. *Soil Mechanics in Engineering Practice.* New York: John Wiley and Sons, Inc.

Vitaletti, A., Cernuto, E., Salciarini, D. 2025. Coupling finite element modelling and InSAR data for enhanced understanding of landslide behaviour along highway infrastructures. *Landslides*, 1-16.

Zhou, W., Li, S., Zhou, Z., Chang, X. 2016. InSAR Observation and Numerical Modeling of the Earth-Dam Displacement of Shuibuya Dam (China). *Remote Sensing*, 8, 877.